Solid Earth, 7, 881–895, 2016
www.solid-earth.net/7/881/2016/
doi:10.5194/se-7-881-2016

Solid Earth Open Access EGU

Structural geology and geophysics as a support to build a hydrogeologic model of granite rock

Lurdes Martinez-Landa[1,3], **Jesús Carrera**[2,3], **Andrés Pérez-Estaún**[4,†], **Paloma Gómez**[5], **and Carmen Bajos**[6]

[1]Department of Civil and Environmental Engineering, Universitat Politècnica de Catalunya (UPC), c/Jordi Girona 1-3, 0803 Barcelona, Spain
[2]Institute of Environmental Assessment and Water Research (IDAEA), CSIC, c/Jordi Girona 18, 08034 Barcelona, Spain
[3]Associated Unit: Hydrogeology Group (UPC-CSIC)
[4]Instituto de Ciencias de la Tierra Jaume Almera, CSIC, c/Lluis Solé Sabaris s/n, 08028 Barcelona, Spain
[5]Centro de Investigaciones Energéticas, Medioambientales y Tecnológicas (CIEMAT), Departamento de Impacto Ambiental de la Energía, 28040 Madrid, Spain
[6]Empresa Nacional de REsiduos (ENRESA), c/ Emilio Vargas 7, 28043 Madrid, Spain
[†]deceased, August 2014

Correspondence to: Lurdes Martinez-Landa (lurdes.martinez@upc.edu)

Received: 6 February 2016 – Published in Solid Earth Discuss.: 22 February 2016
Revised: 19 April 2016 – Accepted: 20 April 2016 – Published: 1 June 2016

Abstract. A method developed for low-permeability fractured media was applied to understand the hydrogeology of a mine excavated in a granitic pluton. This method includes (1) identifying the main groundwater-conducting features of the medium, such as the mine, dykes, and large fractures, (2) implementing this factors as discrete elements into a three-dimensional numerical model, and (3) calibrating these factors against hydraulic data (Martínez-Landa and Carrera, 2006). A key question is how to identify preferential flow paths in the first step. Here, we propose a combination of several techniques. Structural geology, together with borehole sampling, geophysics, hydrogeochemistry, and local hydraulic tests aided in locating all structures. Integration of these data yielded a conceptual model of the site. A preliminary calibration of the model was performed against short-term (< 1 day) pumping tests, which facilitated the characterization of some of the fractures. The hydraulic properties were then used for other fractures that, according to geophysics and structural geology, belonged to the same families. Model validity was tested by blind prediction of a long-term (4 months) large-scale (1 km) pumping test from the mine, which yielded excellent agreement with the observations. Model results confirmed the sparsely fractured nature of the pluton, which has not been subjected to glacial loading–unloading cycles and whose waters are of Na-HCO_3 type.

1 Introduction

Low permeability fractured media have an important role in enhanced geothermal energy and waste management. Studies of this media are hampered by the contrast between conductive fractures and a nearly impervious matrix, and this heterogeneity must be considered. The characteristics and challenges of these media have led to studies in a large number of investigation sites, notably in granites, around the world: Stripa (Rouleau and Gale, 1985; Long et al., 1991), Äspö (Tsang et al., 1996; Svensson, 2001b) and Forsmark (Stephens et al., 2015; Selroos and Follin, 2013) in Sweden; Grimsel in Switzerland (Mauldon et al., 1993; Martínez-Landa and Carrera, 2005); Fanay-Augères in France (Cacas et al., 1990); Mirror Lake in New Hampshire, USA (Shapiro and Hsieh, 1991; Day-Lewis et al., 2000); Olkiluoto in Finland (Ko et al., 2015), and the Canadian Shield (Frape et al., 1984), among others. Most of these sites are located in zones affected by the last glaciation, which caused severe deformation and fracturing. In contrast, sites in southern Europe have not been subjected to glacial unloading stresses. As a re-

sult, most fractures have been driven by much older tectonics (Pérez-Estaún et al., 2002; Escuder-Viruete et al., 2003b) and they have been largely filled by mineral precipitates. In addition, saline water has never infiltrated these systems, so that the deep water is of Na-HCO_3, rather than Na-Cl type. This group of sites includes El Berrocal pluton (Guimerà et al., 1995) or Ratones mine (Martínez-Landa et al., 2004), both of which are in Spain. This article is based on work conducted at the Ratones Mine in Cáceres province of Spain (Fig. 1), and contributes to improve our understanding of this type of media.

There is currently no generally accepted method for modeling low-permeability fractured media. While several different approaches have been used, they are generally combinations of methods of modeling two extremes: continuous medium and discrete fracture networks. Continuous medium fracture network-based approaches assimilate the domain to a porous medium, which includes the effect of fractures. The hydraulic conductivity field is estimated by geostatistical techniques conditioned to actual measurements of hydraulic conductivity and pressure at observation points (Neuman, 1988; Carrera and Heredia, 1988; Gómez-Hernandez et al., 1999; Day-Lewis et al., 2000; Vesselinov et al., 2001; Svensson, 2001a; Ando et al., 2003; Illman and Tartakovsky, 2005; Illman et al., 2009; Illman, 2014; Selroos and Follin, 2013; Ko et al., 2015). Discrete fracture network-based approaches represent the medium by means of fractures networks that are statistically generated. This approach is based on the assumption that fractures behave as preferential flow paths (Dershowitz, 1984; Long and Billaux, 1987; Cacas et al., 1990; Dershowitz et al., 1991; Castaing et al., 2002). More sophisticated fracture network models are channel network models, which represent only the conductive portions of the fractures planes (Moreno and Neretnieks, 1993). We have been using an intermediate mixed approach that treats the matrix and minor fractures as an equivalent, possibly heterogeneous, porous medium and deterministically simulates the hydraulically dominant fractures (Martínez-Landa and Carrera, 2006). The main drawback of this approach is that these dominant fractures must be identified and characterized. Strict characterization is only possible in intensely tested environments. Therefore, the validity of such an approach may be questionable when flow is predicted at longer scales. This is especially worrisome in view of the apparent ubiquity of scale effects.

Scale effects refer to the apparent increase of hydraulic conductivity or transmissivity as rock volume increases (Clauser, 1992; Illman and Neuman, 2000; Vesselinov et al., 2001). Multiple explanations exist for scale effects. Illman (2004) provides a thorough discussion on scale effects and their origin, pointing to other issues such as poorly developed wells (Butler and Healey, 1998) and turbulence in the boreholes (Lee and Lee, 1999). Guimerà et al. (1995) argue that long-term pumping tests are purposefully performed at the most conductive intervals, implying that they are not representative. Other authors (Sánchez-Vila et al., 1996; Meier et al., 1998; Day-Lewis et al., 2000) attribute scale effects to the connectivity among structures. Certainly, the hydraulic conductivity derived from interpreting pulse tests yields information about the closer vicinity of the borehole, which results in marked differences between values associated with intervals that intersect any conductive structure and those that are open only in the matrix (Martínez-Landa and Carrera, 2005). In cross-hole tests, pumping must be performed at intervals in high conductivity zones to maintain a significant flow rate over a long period of time, but pumping also affects points located in the matrix. If the interpretation of the tests does not take into account the existence of conductive fractures, the conductive fractures will lead to a high effective hydraulic conductivity. Martínez-Landa and Carrera (2005) reported that this effective conductivity is appropriate for predicting large-scale tunnel inflows. Such effective conductivity, however, is far larger than the average of any small-scale hydraulic test, the vast majority of which are sparsely fractured; hence, the scale effect occurs.

Thus, good representation of fractured media requires identification of the main water-conducting features. We contend that this is possible by integrating different types of information (geology, geophysics, hydrochemistry, and hydraulics). Accounting for the heterogeneity allows for the use of models for non-trivial predictions under conditions that differ from those during calibration. This has been demonstrated in previous studies (Carrera et al., 1990, 2000; Carrera, 1993), but always at scales similar to those during calibration. Still, the best indicator of model robustness lies in its ability to predict changes in flow conditions at scales different from those during calibration. We propose that structural geology and geophysics can be used to identify large water-conducting fractures that have not been characterized by direct hydraulic tests. By assigning the hydraulic parameters of similar fracture types whose water-conducting fractures have been characterized, we could effectively extend the model scale and potentially model a large volume of rock. This article has three objectives. First, we present a method based on the above proposal and test its predictive capability. Second, we discuss the scale effects observed at the Ratones mine. Finally, we provide additional information regarding the low-permeability fractured media of the Iberian Peninsula in southern Europe. To accomplish these objectives, we analyzed field data sets from the Ratones Mine (study of the hydrogeology around an old uranium mine excavated in a granitic pluton). Data sets were obtained from geochemical, geologic-structural, geophysics, and hydrogeological studies that aided in identifying the main structures (heterogeneities), including their position, direction, dip, and extent. A three-dimensional (3-D) numerical model was then constructed, where the matrix and minor fractures were treated as an equivalent porous medium, and the identified fractures were implemented as 2-D planes embedded in the matrix. This numerical model was then used to calibrate cross-hole

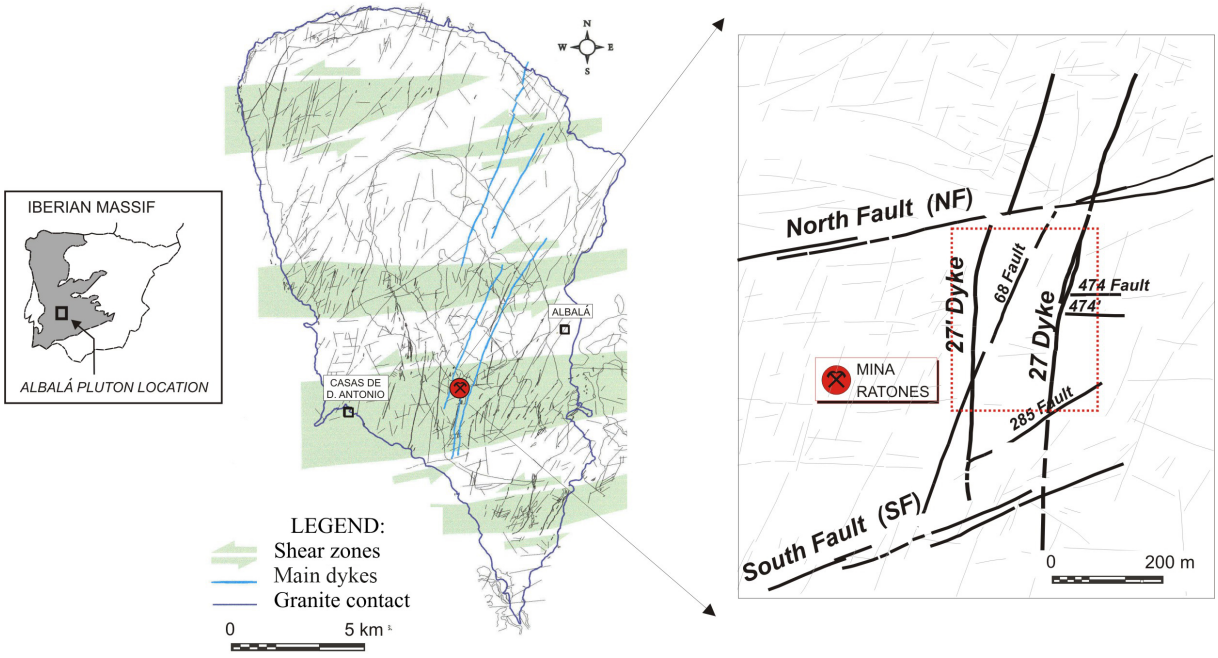

Figure 1. Geological map of Albalá granitic pluton with location of the Mina Ratones area (ENRESA, 1996; Escuder-Viruete and Perez-Estaun, 1998).

tests and to predict the results of long-scale pumping tests from the mine.

2 Test site

2.1 Geological and geophysical characterization

The Albalá granitic pluton is located in the southwest sector of the Iberian Massif (Central Iberian Zone of Julivert et al., 1972). The pluton is a concentrically zoned body, elongated in an N–S direction, with porphyric biotite granites in the rim and fine-grained two-mica leucogranites in the core (Fig. 1). Ratones is an abandoned uranium mine, located in the central aureoles of the pluton. The fault zone architecture in the Mina Ratones area was established on the basis of field geology, structural analysis, seismic experiments, drill cores (Ratones borehole, *Sondeo Ratones*, SR1 to 5) and sonic well log data (Escuder-Viruete and Perez-Estaun, 1998; Carbonell and Pérez-Estaún, 1999; Escuder-Virutete, 1999; Jurado, 1999; Pérez-Estaún, 1999; Jurado, 2000; Martí et al., 2002). Surface geology was mapped at a 1 : 1000 scale in a zone that includes the block where the seismic tomography survey was to be conducted. The resulting maps included granitic facies, dykes, ductile-brittle shears, fault zones, and granitic soil cover (lehm). The 3-D fault distribution obtained for this area is shown in Fig. 2. The post-Variscan structural evolution of the Albalá granitic pluton was established on the basis of fault kinematics and paleostress analysis in superficial outcrops (Escuder-Viruete and Perez-Estaun, 1998; Pérez-Estaún et al., 2002). This evolution includes three episodes of brittle deformations related to different stress-field configurations, which cut and reactivated ductile and ductile-brittle late-Variscan structures.

1. The first episode was extensional and produced the intrusion of Jurassic subvertical diabasic dykes, aligned following a NNE–SSW trend. The constant trend of these dykes at regional scale indicates that $\sigma 3$ was subhorizontal and WNW–ESE to NW–SE directed.

2. The second episode was characterized in the Mina Ratones area by the development of strike-slip faults with E–W direction and kilometer thickness.

3. The third fracturation episode, post-Hercinian, partially reactivated the previous WSW–ENE to E–W structures and dykes as normal and normal-slip faults (Escuder-Viruete and Perez-Estaun, 1998; Pérez-Estaún et al., 2002).

The main identified structures in the Ratones area (Figs. 1 and 2) are as follows.

The North Fault (NF) has a N70 to N80° E trend and a 55–65° S dip, diminishing with depth to 30–40°.

The South Fault (SF) has a N64 to N78° E trend and a 68–82° N dip. It has a subvertical set of parallel fractures, forming a fragile transcurrent shear zone.

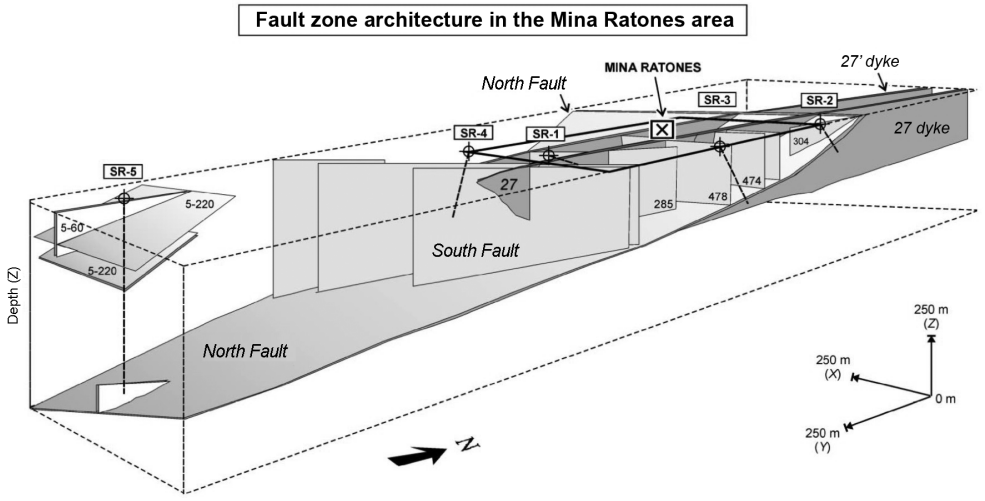

Figure 2. Fault zone architecture of Mina Ratones area obtained from structural, seismic, core, and well log data (Escuder-Viruete and Perez-Estaun, 1998; Carbonell and Pérez-Estaún, 1999; Escuder-Virutete, 1999; Pérez-Estaún, 1999; Escuder-Viruete et al., 2001). The main identified structures are the North Fault (NF), the South Fault (SF), and the 27 and 27' dykes. Other relevant brittle structures of minor size are faults 474 and 285.

The 27 and 27' mineralized subparallel and subvertical dykes have a thickness of 0.4–1.8 m, are composed of a quartz breccia, and are cemented by sulfides (Escuder-Viruete et al., 2003a, b).

The damage zone is defined by small faults and kinematically related fracture sets and joints. The dykes and other fractures (as NF and SF) are hosted in an extensively fractured damage zone of hydrothermally altered granite (fractured belts).

Other relevant brittle structures of minor size include the following.

The 474 and 474' faults are two high-dip subparallel structures that trend N64 to N76° E. Both structures connect toward the W with the 27 dyke.

The 285 brittle structure is also a sinistral strike-slip fault with a N52 to N60° E trend and subvertical dip. Faults 474 and 285 are younger than the NF; they cut and displace it, so that it remains hydraulically disconnected.

The last deformational phase indicates that the stress state at the recent evolution was in a E–W direction. As a result, the north and south family fractures are oriented in the most favorable direction, making them ideal candidate water-conducting structures. For the purpose of subsequent hydrogeological analyses, it is important to highlight that (1) the above discussion is the result of a structural geological interpretation of 3-D seismics. (Specifically, direct seismic inversion was often modified after discussions with structural geologists, who pointed to inversion inconsistencies. Therefore, it can be stated that seismic inversion was "structural geologically biased".) (2) Some water-conducting faults (specifically 474, and 285) were identified during seismic inversion, but had not been mapped because they are located in an area covered by meadows. (3) Geophysics also helped to identify highly fractured zones (e.g., fractured granitic units, fractured belts around the dykes and the South Fault), which provided hydraulic connectivity.

2.2 Hydrogeochemical characterization

Rainwater entering into the rock-mine system is saturated with atmospheric O_2, leading to (1) oxidation of metal sulfides present in the dykes and mineralized fractures, (2) precipitation of metal oxyhydroxides, and (3) the addition of acid to the medium. Acidic water causes dissolution of carbonates in fissure fillings, buffers the mine water pH, and promotes the precipitation of metals released by sulfide oxidation as metal carbonates (Fig. 3). In parallel, plagioclase weathering promotes kaolinite precipitation in the shallower areas. The albite becomes smectite clay, resulting in sodium bicarbonate waters in the deeper areas (400–500 m deep, borehole SR5) with transit times of tens of thousands of years (16 000 years dated with noble gases). These sodium bicarbonate waters are typical of granitic water with relatively high residence times. The groundwater circulating through granites in the Hesperian Massif is of sodium bicarbonate type, which may be significant for waste disposal in this type of rock (Gómez, 2002; Gómez et al., 2006). This is different from the chemical composition of the groundwater in granitic formations in other parts of the world, such as in the Hercinian granitic in the Chardon U mine in France (Beaucaire et al., 1999) and in the Canadian (Frape et al., 1984)

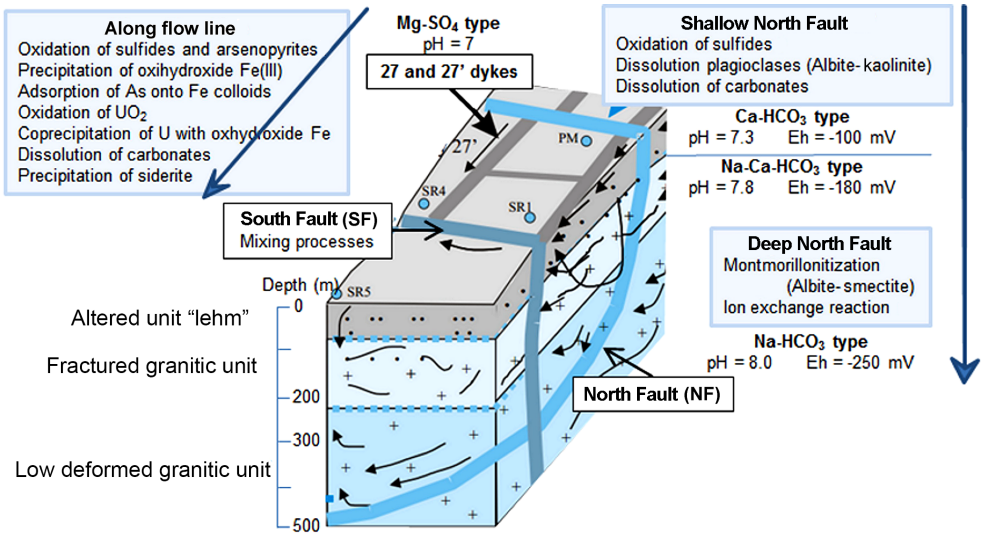

Figure 3. Groundwater hydro-geochemical behavior model of the Ratones aquifer-mine system (modified from Gómez, 2002).

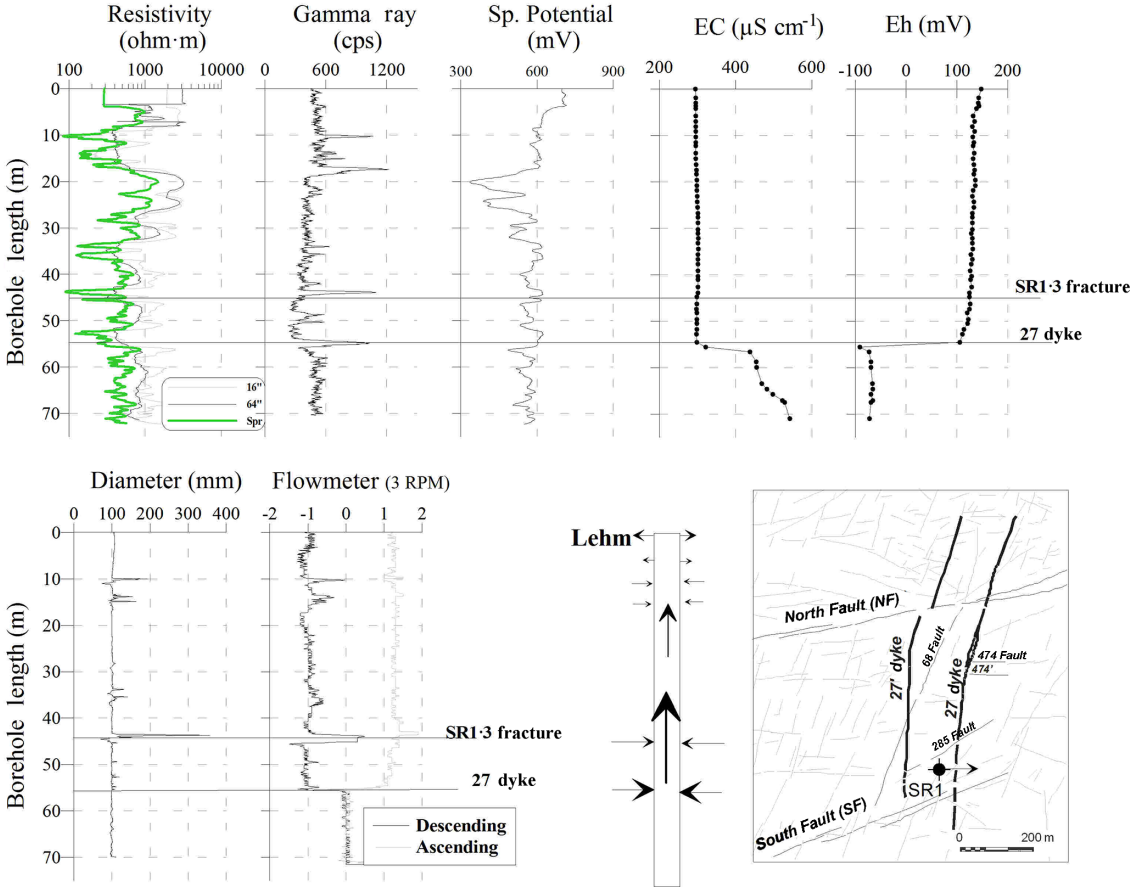

Figure 4. Some of the chemical and geophysical logs recorded at borehole SR1, which helped to identify dyke 27 and fracture SR1-3. The chemical logs only display the effect of dyke 27, because all upper water (including SR1-3) is mine water. The effect of both structures can be noticed in other logs, especially in the gamma log, due to the fracture filling. Flowmeter values, recorded with an upward flow rate of pumping indicate little water flow beneath dyke 27. The same applies to a lesser extent to fracture SR1-3.

and Scandinavian (Blomqvist, 1999) shields, where chloride and sodium are the major ions. Hydrogeochemical studies help to identify water-conducting fractures. Water flowing through fractures is chemically marked by water–rock interactions along the flow path within the medium (Perez del Villar et al., 1999; Gómez et al., 1999, 2001; Gómez, 2002). This enables the identification of some fractures and potential connections. Figure 4 shows an example of the downhole geophysical loggings and records of a multiparametric device (electrical conductivity, redox potential, resistivity, gamma rays, spontaneous potential, diameter, and flowmeter) in borehole SR1, down-gradient of the mine. These data were used to identify the intersection with dyke 27, where water flows from the mine, as indicated by chemical parameters and changes in the upward velocity of flow within the borehole (flowmeter log).

2.3 Hydraulic characterization

As discussed above, geology and geophysics provide insight into the physical configuration of the fracture network. Structural geology and geochemistry help to identify which of those fractures may be water-conducting. Simple borehole hydraulic tests (pulse tests, slug tests, and constant head tests) provide the location of these structures and their hydraulic conductivity. Large-scale connectivity can be identified using cross-hole tests and hydrochemistry if the water contains a chemical tracer. The hydraulic conceptual model of the system is largely based on the hydraulic extent of the fractures and their connectivity, which is why a hydraulic testing survey was designed. Different types of measurements were used.

a. Development pumping was carried out in all SR boreholes, comprising pumping with an open borehole to withdraw all drilling materials.

b. Chemical sampling pumping was carried out of NF in borehole SR2, of SF in borehole SR4, and some intervals of SR5. Time, flow rate, and interval pressure were measured. These data were used as hydraulic test data.

Additionally, specifically designed hydraulic tests were conducted.

c. Pulse, slug, and constant head single-hole tests were conducted at short intervals in boreholes SR3, SR4, and SR5. The three tests were performed between two packers separated at a constant distance and a system of pipes and valves to allow the injection or extraction of very low water volumes with high precision (Ortuño et al., 2000).

d. Three cross-hole tests were planned. For this purpose, the boreholes were divided into intervals and hydraulically isolated by packers. The position of the packers was determined to isolate the structures that had to be tested. Each interval was equipped with a pressure outlet and a water injection/extraction point.

d1. The North test had a pumping interval of S14-1 (first interval of S14 borehole, numbered from bottom to top) which was designed to characterize the dyke 27 up-gradient of the mine.

d2. The East test had a pumping interval of SR3-1, which intersects the NF, like SR2-2. After pumping for 9 days, there were no responses at any observation point. Interpretation of the seismic profiles in a subsequent stage (Pérez-Estaún, 1999; Martí et al., 2002) revealed the absence of a possible hydraulic connection between these points because the NF was cut and displaced by faults 474 and 285 (see Fig. 2).

d3. The South test had a pumping interval of SR4-1. This was located in the discharge zone of the mine, pumping within the SF. This was the only test in which all observation points reacted to the pumping.

Hydraulic characterization begins with a single-hole test (pulse, slug, and constant head). The calibrated parameters provide insight into the transmissivity field around the boreholes, and allow for identification of the most conductive intervals. Cross-hole tests were then conducted in these boreholes to identify connectivities. All hydraulic tests were interpreted using the Theis method (Theis, 1935). This model assumes that the medium is homogeneous and isotropic, thereby integrating the effect of heterogeneities into the matrix. In cross-hole tests, the preliminary interpretations were done separately for each recorded drawdown curve, which yielded a couple of transmissivity–storage (T-S) values for each observation point (Fig. 5). Note that estimated Ts range over 1 order of magnitude, whereas the estimated S's, which are presumed nearly constant, range over almost 5 orders of magnitude. These highly variable storativities provide information about the connectivity between pumping and observation points through fractures. A good connection is reflected by a fast response (i.e., high diffusivity, T/S). As discussed in the introduction, the estimated T reflects large-scale conductivity. Therefore, the estimated storage coefficient will be low for observation points that are well connected to the pumping interval (Meier et al., 1998). The dykes and NF and SF are accompanied by systems of minor fracturing that form part of a higher transmissivity zone situated around these structures. Points S10 and SR1-3, which display the lowest S values (Fig. 5), are connected to the pumping point through these fracturing belts. In the 3-D numerical model, this connectivity was simplified by simulating fracture planes referred to as fracture S10 to connect point S10 to the pumping interval SR4-1, and fracture SR1-3 to connect point SR1-3 to SR4-1. The remaining observation points have a lower response (i.e., higher S) to the pumping.

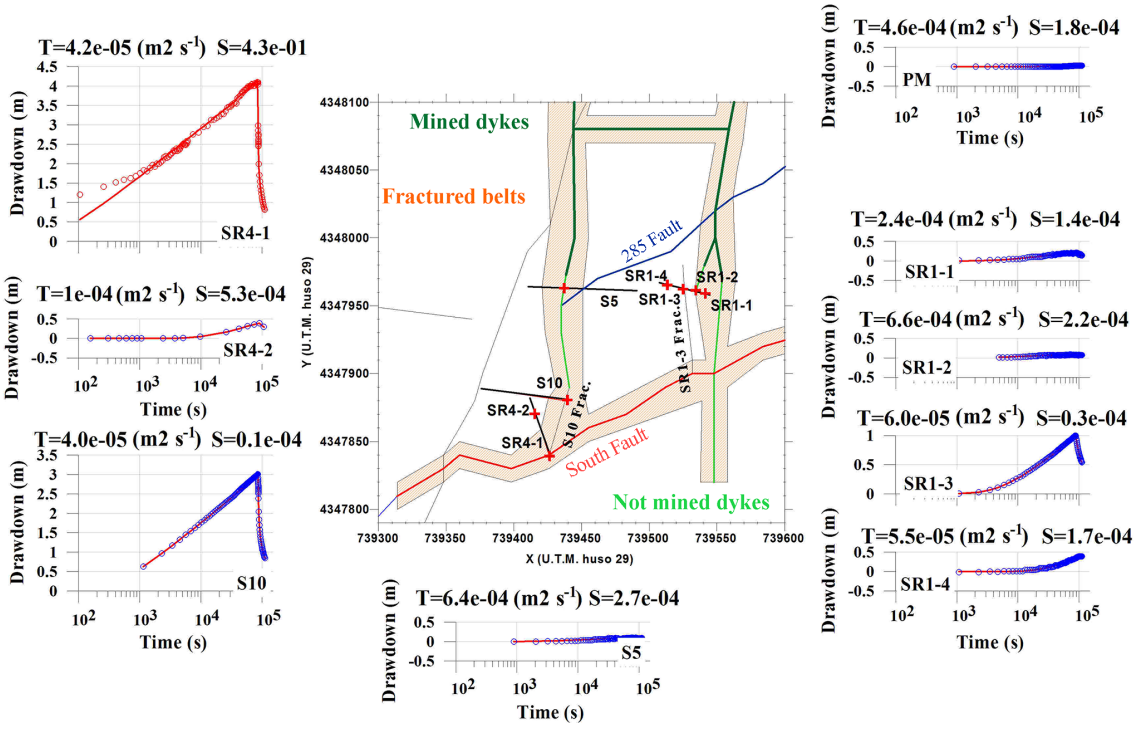

Figure 5. Results from preliminary interpretation of the South cross-hole test (pumping at SR4-1). Transmissivity and storativity are derived by fitting each borehole drawdowns, one at a time, using the Theis model. The degree of connectivity was derived from the estimates of storage coefficients. T varies from 4 to 64 $\times 10^{-5}$ m^2 s^{-1}, while S ranges from 1 $\times 10^{-7}$ to 0.43. We take S estimates to reflect connectivity. A small S (fast response) implies a good hydraulic connection between pumping and observation wells. This suggests that the best connections occur between the pumping interval and points S10 and SR1-3, while points S5 and SR1-2, and, especially mine well (point PM, Pozo Maestro), were damped by the mine influence (which behaves as a constant head boundary).

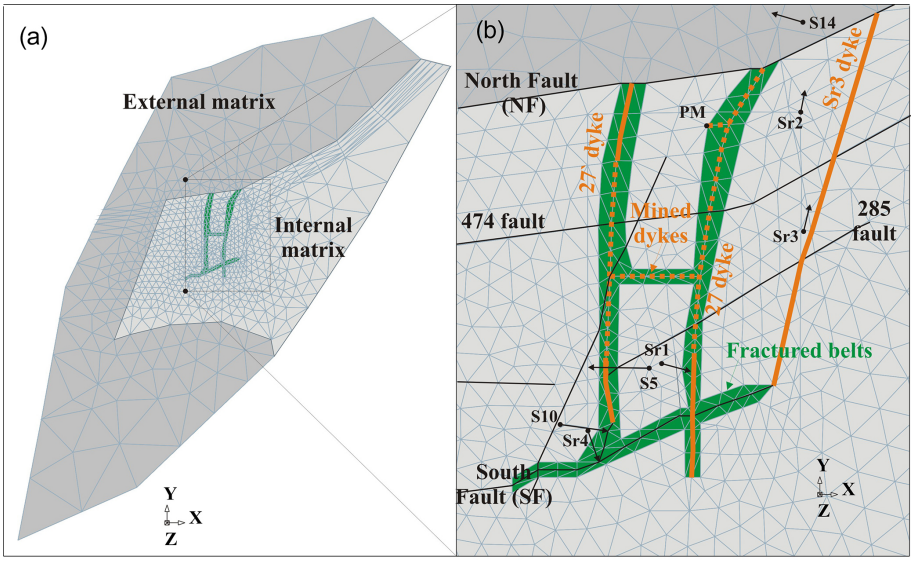

Figure 6. Model geometry. The model comprises two areas. The external matrix area is treated as an equivalent porous media without explicit fractures, because not all of the main structures have been identified. At the local level (right picture), the main structures are explicitly taken into account, including the fractures, dykes 27, 27', and SR3, and the mine itself, which is excavated in both dykes. The structures are represented by means of 2-D elements. The Maderos creek is embedded in the SF. Projections of the boreholes that are closer to the mine are represented by black dots on the surface and by an arrow pointing to the borehole end.

Observation points S5 and SR1-2 intersect dykes 27' and 27, respectively. A priori, these should have a better response to the pumping. Drawdowns between both points were limited by the influence of the mine cavity, which acts as a constant head boundary.

3 Numerical model

A 3-D numerical model was constructed to interpret the South cross-hole test, taking into account the water-conducting features. Figure 6 displays a plan view of the features introduced in the model. The granitic matrix was divided into two zones depending on the degree of characterization of the whole area. On the one hand, the internal matrix represents, in detail, all the fractures identified around the mine. On the other hand, the external matrix does not include all of the structures (because they have not all been identified). The external matrix has larger hydraulic conductivities than the internal matrix, because it includes the effect of the unidentified fractures. Its value was assigned by approximately evaluating the effective hydraulic conductivity (matrix plus fractures) of the area that was characterized in detail. The model reaches up to 600 m depth to include all measurements (the SR5 borehole reached a depth of 500 m) and all units. The shallowest layer is formed by 2-D elements and represents the lehm, which comprises altered, disaggregated, and washed granite (much like granitic sand) with high hydraulic conductivity. This layer drains rapidly in humid seasons, and carries no water in dry seasons. The altered unit reaches a depth of 20 m according to geophysics and borehole samples. The layer is highly weathered, but the granite structure is conserved. Its hydraulic conductivity and porosity are higher than those of unaltered granite due to the decomposition of feldspar. The fractured granitic unit could be identified by geophysics, and corroborated by the hydraulic characterization of a borehole 500 m deep (Fig. 7) that was drilled in the matrix far from the mine. At this depth, hydraulic conductivity is reduced, and remains almost constant up to this horizon. In this unit, the granite does not behave like the altered unit, but its fracturing index is high and, therefore, its effective hydraulic conductivity is higher than that of non-deformed granite. Finally, the non-deformed granitic unit, in contrast to the other units, has a lower fracturing index and effective hydraulic conductivity. Both the matrix effective hydraulic conductivity and specific storage decrease with depth. The upper units (lehm and altered granitic unit) are treated as separate hydraulic conductivity zones. Constant hydraulic conductivity is also adopted in the bottom portion of the model (below 350 m; Fig. 7). The linear relationship proposed by Stober (1997) was adopted between the upper and lower units. Storativity drops linearly by an order of magnitude between the surface and the bottom (600 m deep), based on the results obtained from the hydraulic tests.

The magnified image in the central part of the model (Fig. 6, right) shows the structures included explicitly in the model. Both matrix zones and fractured belts are simulated by 3-D elements; fractures are reproduced with 2-D elements (lines in the figure); finally, boreholes are introduced as 1-D elements (points in the figure). Structures included in the model (Fig. 8) through 2-D elements preserve their azimuth, dip, and interception points with the boreholes. In general, they are subvertical, except for the NF, which is slanted on the surface and cut, displaced, and tilted by fractures 474 and 285. The mine is also treated with 2-D elements, because it corresponds to the mining of part of dykes 27 and 27' (planar structures).

3.1 Model calibration of the cross-hole South test

Once the conceptual model was built and the numerical model implemented, a cross-hole test conducted downstream of the mine (South test) was calibrated. As initial parameters, those obtained from interpretation of the test with the Theis model were taken. The interpretation model of the south cross-hole test works with drawdowns; that is, initial drawdowns were zero and all prescribed fluxes, except the pumping, were set to zero. The model boundaries were placed at a distance large enough to impose a zero drawdown condition. Table 1 summarizes the results obtained alter calibrating the test. Note that fully penetrating boreholes are explicitly included in the model to represent that they connect fractures.

Figure 9 represents the resulting model fits. The pumping point is SR4-1, intercepting the SF. Observation points S10 and SR1-3 respond rapidly to the stress, because they are connected to the pumping point through small structures that form the fractured belts (simplified in the model as fracture S10 and fracture SR1-3), which intercept the SF. The remaining observation points were not that well connected with the pumping point. Pozo Maestro (PM) is the mine well, whose response (changes in pressure due to the injection test, represented as drawdowns) is to completely damp the poor connection with the pumping point. Observation points S5 and SR1-2 cut dyke 27' and 27, respectively, close to the mine. The pumping withdraws the water mainly from the shallow layer (lehm), draining it through the bed of Maderos stream, where water flows sub-superficially. Water also comes from the mine and the altered granitic unit, flowing towards the pumping point through the fractures (SF, fractured belts, and dykes).

4 Scale effect

Figure 10 represents the hydraulic conductivities obtained from all hydraulic tests as a function of the scale. Transmissivities derived from the tests are divided by the length of the pumped interval to convert them into conductivities. The scale of the test is determined by the rock volume af-

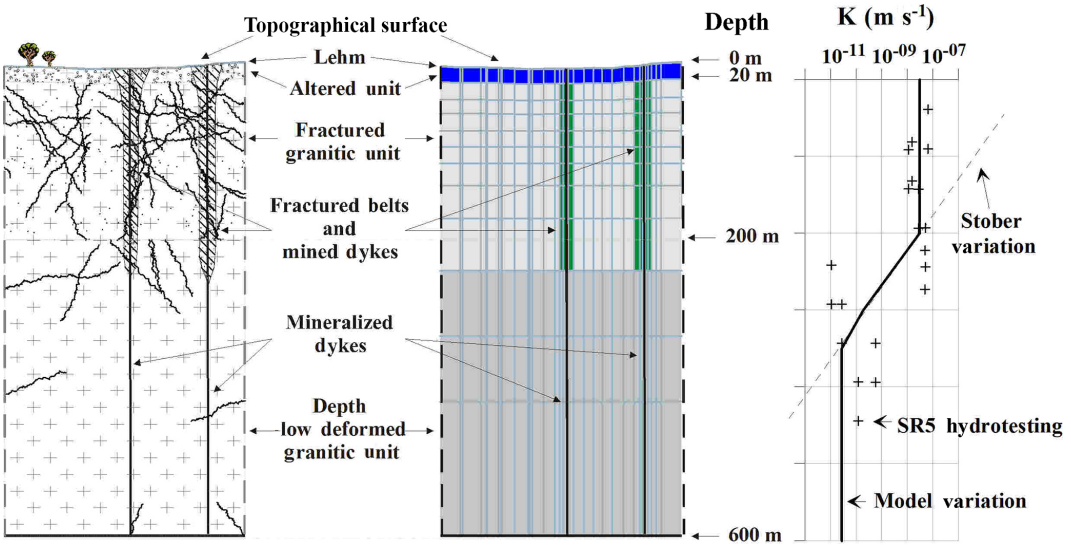

Figure 7. Schematic vertical section representing variations in data derived from the hydraulic characterization of borehole SR5 (500 m deep) indicate that hydraulic conductivity changes with depth. This fact was studied by Stober (1997). The model uses a modification of Stober's equation: hydraulic conductivity is kept constant up to the base of the fractured granitic unit (200 m), then changes with depth down to 350 m. From there, it remains constant down to the model bottom.

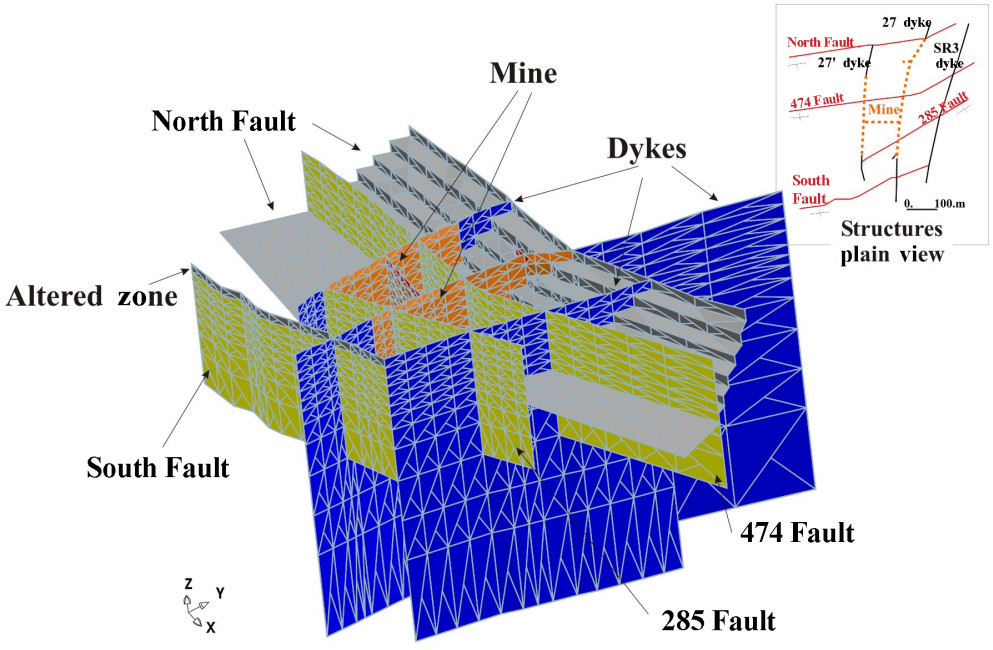

Figure 8. Main structures implemented in the model as planar structures. They are defined by 2-D elements. The model honors surface traces and dips. Downwards extension of these structures is performed with the aid of geophysics, structural geology, and intersections at boreholes. The NF is the more vertical one at its upper section, and it is cut and disconnected by faults 474 and 285 towards the south. The mine is also represented by means of 2-D elements, because it results from the exploitation of the dykes. The SF is zonated at the surface, in order to reproduce the altered zone in which the stream is embedded, where most of the water flows.

fected by each test, which ranges between a few centimeters (pulse tests) to some tens of meters (South cross-hole test). As mentioned above, the tested intervals did not coincide for all types of tests. In the case of pulse, slug, and constant head tests, they were conducted sequentially with the same interpretation, but they do not coincide with the packed off inter-

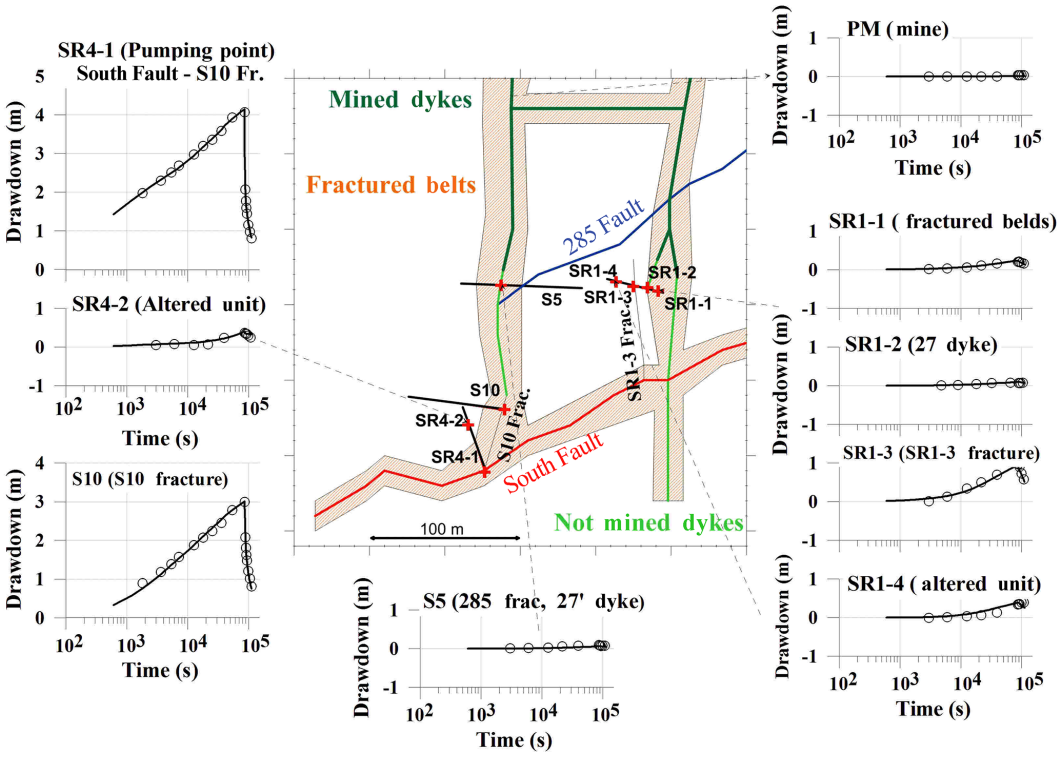

Figure 9. Results obtained after calibrating the SR4-1 cross-hole test are indicated by a black line; observed data are indicated with circles using a 3-D model. All graphs maintain the vertical scale to facilitate comparison of the results.

Table 1. Parameters obtained after calibrating the South cross-hole test. Units are meters and seconds, 1-D features are defined in terms of hydraulic conductivity and specific storativity by assigning them a 1 m^2 cross-sectional area. Hydraulic conductivity values of matrix and fractured belts change with depth: the first value holds for the upper 250 m (constant parameter), the second value applies to the bottom of the domain – both for the matrix and the fractured belts. The storativity of the fractured belts lehm is negligible in the model (1.0×10^{-30}), to prevent the artifact that water might be withdrawn from that zone. Standard deviations (SDs) of the decimal logarithms of estimated parameters (not shown for parameters held constant during calibration) are also presented as a measure of uncertainty.

Parameters (m and s)	Dim.	T ($m^2\,s^{-1}$)	K ($m\,s^{-1}$)	SD (T/K)	S (–)	Ss (m^{-1})	SD (Ss/S)
Matrix	3-D		2.1×10^{-10} / 7.7×10^{-14}	0.16		1.1 × 10-8	0.16
Fractured belts	3-D		1.5×10^{-8} / 1.5×10^{-10}	0.07		1.10 × 10-7	0.09
Mined dykes	2-D	0.1		–	2.7×10^{-3}		–
Dykes	2-D	6.4×10^{-7}		0.044	1.0×10^{-7}		–
S10 fracture	2-D	1.07×10^{-5}		0.039	1.0×10^{-7}		–
285 fracture	2-D	2.0×10^{-5}		0.17	1.0×10^{-7}		–
South Fault	2-D	1.9×10^{-5}		0.012	1.0×10^{-7}		–
SR1-3 fracture	2-D	1.1×10^{-6}		0.086	1.0×10^{-7}		–
Lehm	2-D	1.9×10^{-5}		0.16	3.6×10^{-3}		0.13
South Fault – Maderos stream	2-D	1.8×10^{-7}		0.18	1.7×10^{-4}		0.026
S10 borehole	1-D		1	–		4.3×10^{-6}	–
S5 borehole	1-D		1	–		4.3×10^{-6}	–
SR4-2 borehole	1-D		1	–		4.3×10^{-6}	–
Altered unit	3-D		2.6×10^{-9}	–		4.3×10^{-7}	0.061
Fractured belts lehm	2-D	1.9×10^{-4}		0.18	1.0×10^{-30}		–

Figure 10. Permeability values obtained from interpretation of hydraulic tests performed at varying scales in different holes and intervals. In general, permeability increased with the increase in scale, except for the cross-hole test, which was performed in the highly transmissive portion of the site. See the text regarding the surprising lack of high K observation during small-scale tests.

vals for the cross-hole tests, which were selected to isolate the main structures from the matrix and minor fractures. It is still possible, however, to compare the calibration parameters with the results of homogeneous and isotropic models (interpreted before using the Theis model), as larger scale tests also involve the rock volume of lower scale tests. The dispersion of hydraulic conductivity values for each test diminished with the scale, because when the medium is treated as homogeneous, it includes the hydraulic conductivities of the main structures in the effective conductivity; i.e., it is more homogeneous. The right panel of Fig. 10 shows the hydraulic conductivity values obtained after interpreting the South cross-hole test with a 3-D numerical model. This 3-D model represents the main features of the medium heterogeneity in an explicit way (fractures, mine, and different units of the granite, depending on its hydraulic behavior). The points represented in Fig. 10, for this cross-hole test, do not represent different results at different observation points, but rather the conductivity of the main fractures, fracturing belts, altered unit, lehm, and matrix. The fracture transmissivities were transformed into conductivities by assigning them a unitary width (dividing by interval lengths). This results in larger conductivity values for the fractures and dykes, whereas the lower values correspond to the matrix elements whose conductivity depends on the fracturing index. The most surprising feature of Fig. 10 is the absence of high conductivity values for small-scale tests. Even if effective permeability increases with scale, some high permeability values should have been identified by the small-scale tests coinciding with the intersection of the fractures that dominate the large-scale behavior of the site (see e.g., Martínez-Landa and Carrera, 2006). We attribute this absence to the fact that characterization tests were performed during an unusually rainy season. The most permeable zones are located at the discharge zone of the mine, which caused some of the boreholes to become flowing wells, making it impracticable to perform a short-scale test for the highest permeable part. As a consequence, the highest values are not available for the short-scale tests. In summary, the lower values of hydraulic conductivity are associated with pulse tests for points situated within the matrix. These values are consistent with the conductivity estimated for the matrix in a 3-D heterogeneous model. The increase in hydraulic conductivity with scale is caused by the contribution of fractures to the effective conductivity obtained when interpreting the tests using homogeneous models.

5 Blind prediction

A 4-month pumping test from the mine was carried out with a mean flow rate of $0.0025\,m^3\,s^{-1}$. All boreholes were used as observation points (Fig. 11). As for the interpretation of the south cross-hole test, all observations were introduced as drawdowns calculated from the measurements registered prior the start of the pumping (assuming steady state). The model adopted the calibrated parameters of the analysis of the South cross-hole test (shown in Table 1), and those ob-

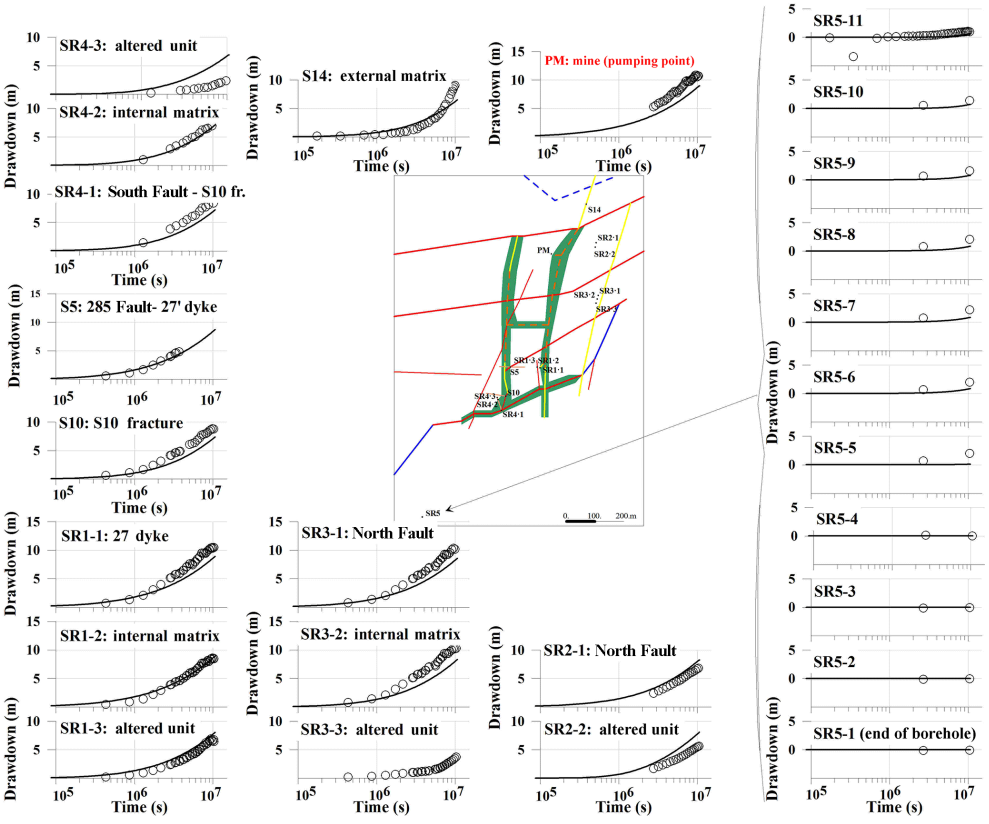

Figure 11. Blind prediction of the long-term pumping of the mine (point PM), using calibrated with the SR4-1 cross-hole test. This pumping lasted for 4 months, and its effects reached all observation points. Measurements are represented by circles, and model results are represented by continuous line.

tained from the hydraulic characterization of structures not involved in the cross-hole tests. Fractures not affected by any test were assigned the transmissivities that had been obtained during calibration for fractures belonging to the same family, according to the geophysical and structural analysis. Specifically, fractures 474, and Fr4 were assigned the values obtained for fracture 285, and the SR3 dyke was assigned the transmissivity obtained for the non-mined portion of the 27 dyke. Results of the blind prediction (i.e., without calibration) are shown in Fig. 11. Overall, the fit of this blind prediction was visually excellent. Nevertheless, it becomes apparent that the estimated specific yield for the south cross-hole test model was too high, which may reflect the fact that the hydraulic characterization of the zone was performed entirely during the winter and within a wet interannual cycle, so that the entire zone was fully saturated. In the prediction, it can be observed that most of the water came from the lehm, which is a very conductive layer with a relatively high specific yield (3.6×10^{-3}), while the altered unit specific yield was set at $4.6 \times 10^{-6}\,\mathrm{m}^{-1}$. This artifact reflects that water is withdrawn from the altered unit, which is the actual storage unit in dry periods. It is worth pointing out the good quality of the responses obtained at intervals SR2-1, SR2-2, SR3-1, and SR3-2, which would have displayed a much more delayed response than observed and modeled data (perhaps similar to the response observed in SR4-3 or SR3-3) if the untested (and only observed through geophysics) fractures had not been included. Perhaps more important, the slope of the late time drawdown in semi-log is quite accurate in most observation points, which suggest that the overall parameters are adequate for this test, even though it lasted some 100 times longer than the calibration tests.

6 Conclusions

The main objective of this work was to show that structural geology and geophysical techniques together with hydrochemical and hydraulic data can help to identify the main fractures, which carry most groundwater flow. Values of transmissivity were estimated at different scales by considering the medium as homogeneous. When plotting these values against the representative field scale, we observed a progressive increase in transmissivity with an increase in scale. This scale effect is attributed to the main fractures because all observations can be explained by incorporating such dominant fractures explicitly into the model. In fact, this model yielded

an excellent fit to a 4-month long pump test that provoked responses at all observation points. The fact that the results of such a long pump test could be blindly predicted using only short-term (< 1 day) tests supports both the use of seismic geophysics and structural geology to identify the dominant fractures and their explicit incorporation into the groundwater flow model (mixed approach). The results are consistent with the hypothesis that southern European granite plutons display low hydraulic conductivity. This, together with the low aggressivity of their sodium bicarbonate groundwater, makes them appropriate for hosting nuclear waste.

Acknowledgements. This work was part of a multidisciplinary project funded by ENRESA (Spanish Nuclear Waste Management Company), through grant no. 770071. Participating institutions included AITEMIN (in charge of hydraulic testing), CIEMAT (chemical sampling), and CSIC-IJA (structural geology). The revised text has benefited from constructive criticism by Christopher Juhlin and Paul Hsieh.

Edited by: F. Bastida

References

Ando, K., Kostner, A., and Neuman, S. P.: Stochastic continuum modeling of flow and transport in a crystalline rock mass: Fanay-Augères, France, revisited, Hydrogeol. J., 11, 521–535, doi:10.1007/s10040-003-0286-0, 2003.

Beaucaire, C., Gassama, N., Tresonne, N., and Louvat, D.: Saline groundwaters in the hercynian granites (Chardon Mine, France): geochemical evidence for the salinity origin, Appl. Geochem., 14, 67–84, doi:10.1016/S0883-2927(98)00034-1, 1999.

Blomqvist, R.: Hydrogeochemistry of deep groundwaters in the central part of the Fennoscandian shield, Helsinki University of Technology (Espoo, Finland) GEOLOGICAL SURVEY OF FINLAND, Nuclear Waste Disposal Research, Report YST-101, http://tupa.gtk.fi/julkaisu/ydinjate/yst_101.pdf, 1999.

Butler, J. J. and Healey, J. M.: Relationship Between Pumping-Test and Slug-Test Parameters: Scale Effect or Artifact?, Ground Water, 36, 305–312, doi:10.1111/j.1745-6584.1998.tb01096.x, 1998.

Cacas, M. C., Ledoux, E., de Marsily, G., Tillie, B., Barbreau, A., Durand, E., Feuga, B., and Peaudecerf, P.: Modeling fracture flow with a stochastic discrete fracture network: calibration and validation: 1. The flow model, Water Resour. Res., 26, 479–489, doi:10.1029/WR026i003p00479, 1990.

Carbonell, R. and Pérez-Estaún, A.: Estudios geológico-estructurales y geofísicos. Tomo II: Caracterización sísmica del entrono de mina Ratones, Internal report: 10·cja·if·03, ENRESA, 1999.

Carrera, J.: Chemistry and Migration of Actinides and Fission Products An overview of uncertainties in modelling groundwater solute transport, J. Contam. Hydrol., 13, 23–48, doi:10.1016/0169-7722(93)90049-X, 1993.

Carrera, J. and Heredia, J.: Inverse modeling of the Chalk River Block, Hydrocoin level 2/case 5a, Nagra TB 88-14, http://www.nagra.ch/en/cat/publikationen/technicalreports-ntbs/ntbs-1987-1988/downloadcentre.htm (last access: 11 May 2016), 1988.

Carrera, J., Heredia, J., Vomvoris, S., and Hufschmied, P.: Modeling of flow with a small fractured monzonitic gneiss block, in: Hydrogeology of low permeability environments, International Association of Hydrogeologist, edited by: Neuman, S. and Neretnieks, I., Hannover, Heise, vol. 2, 115–167, 1990.

Mixed discrete-continuum models: a summary of experiences in test interpretation and model prediction, Dynamics of Fluid in Fractured Rock, Geophysical Monograph, AGU, edited by: Faybishenko, B.,Whiterspoon, P. A., and Benson, S. M.,available at: http://onlinelibrary.wiley.com/doi/10.1029/GM122p0251/summary, 2000.

Castaing, C., Genter, A., Bourgine, B., Chilès, J., Wendling, J., and Siegel, P.: Taking into account the complexity of natural fracture systems in reservoir single-phase flow modelling, J. Hydrol., 266, 83–98, doi:10.1016/S0022-1694(02)00114-2, 2002.

Clauser, C.: Permeability of crystalline rocks, Eos, Transactions American Geophysical Union, 73, 233–238, doi:10.1029/91EO00190, 1992.

Day-Lewis, F. D., Hsieh, P. A., and Gorelick, S. M.: Identifying fracture-zone geometry using simulated annealing and hydraulic-connection data, Water Resour. Res., 36, 1707–1721, doi:10.1029/2000WR900073, 2000.

Dershowitz, W.: Rock Joint System, PhD thesis, Massachusetts Institute of Technology, Cambridge, https://dspace.mit.edu/handle/1721.1/27939#files-area, 1984.

Dershowitz, W., Wallmann, P., Geier, J., and Lee, G.: Discrete fracture network modeling of tracer migration eexperiment at the SCV site, SKB Report 91-23, Swedish Nuclear Power and Waste Management Co, Stockholm, Sweden, 1991.

ENRESA: Memoria cartográfica geológica y estructural. Rocas Plutónicas, Albalá (G111), Internal Report: 94·G111·IF Vol. II, ENRESA, Madrid, Spain, 249 pp., 1996.

Escuder-Viruete, J. and Perez-Estaun, A.: Fracturacion en Mina Ratones. Informe Final 1: Estructura, Proyecto Ratones, ENRESA, internal report, 10·cja·if·01, ENRESA, 1998.

Escuder-Viruete, J., Carbonell, R.and Jurado, M., Marti, D., and Perez-Estaun, A.: Two dimensional geostatistical modeling and prediction of the fracture system in the Albala Granitic Pluton, SW Iberian Massif, Spain, J. Struct. Geol., 23, 2011–2023, doi:10.1016/S0191-8141(01)00026-8, 2001.

Escuder-Viruete, J., Carbonell, R., Martí, D., and Pérez-Estaún, A.: 3D stochastic modeling and simulation of fault zones in the Albalá granitic pluton, SW Iberian Variscan Massif, J. Struct. Geol., 25, 1487–1506, doi:10.1016/S0191-8141(02)00183-9, 2003a.

Escuder-Viruete, J., Carbonell, R., Martí, D., Jurado, M., and Pérez-Estaún, A.: Architecture of fault zones determined from outcrop, cores, 3D seismic tomography and geostatistical modeling: example from the Albalá Granitic Pluton, SW Iberian Variscan Massif, Tectonophysics, 361, 97–120, doi:10.1016/S0040-1951(02)00586-3, 2003b.

Escuder-Virutete, J.: Estudios geológico-estructurales y geofísicos. Tomo I: Estudios geologicos, Internal report: 10·cja·if·03, ENRESA, Madrid, Spain, 1999.

Frape, S., Fritz, P., and McNutt, R.: Water-rock interaction and chemistry of groundwaters from the Canadian Shield,

Geochim. Cosmochim. Ac., 48, 1617–1627, doi:10.1016/0016-7037(84)90331-4, 1984.

Gómez, P.: Estudio del impacto de la mina de uranio "Los Ratones" (Albalá, Cáceres) sobre las aguas superficiales y subterráneas: modelación hidrogeoquímica., PhD thesis, Universidad Autónoma de Madrid, Madrid, 2002.

Gómez, P., Garralón, A., Turrero, M., Sánchez, L., Melón, A., Ruiz, B., and Fernández, F.: Impacto ambiental de la restauración de la Mina Ratones en las aguas subterráneas., Internal report, 10·cie·if·1·99, ciemat/diae/54211/7/99, ENRESA, 1999.

Gómez, P., Garralón, A., Turrero, M., Sánchez, L., Ruiz, B., and Melón, A.: Estudio del efecto de la restauración de la Mina Ratones en las aguas subterráneas, Internal report, 10·cie·if·1·00, ciemat/diae/54440/1/00, ENRESA, 2001.

Gómez, P., Turrero, M., Garralón, A., Peña, J., Buil, B., De la Cruz, B., Sánchez, M., Sánchez, D., Quejido, A., Bajos, C., and Sánchez, L.: Hydrogeochemical characteristics of deep groundwaters of the Hesperian Massif (Spain), J. Iber. Geol., 32, 113–131, 2006.

Gómez-Hernandez, J., Hendricks Franssen, H., Shauquillo, A., and Capilla, J.: Calibration of 3D transient groundwater flow models for fractured rock., in: Proceedings Model Care'99, International Conference on Calibration and reliability in groundwater modeling, Zurich, 1999.

Guimerà, J., Vives, L., and Carrera, J.: A discussion of scale effects on hydraulic conductivity at a granitic site (El Berrocal, Spain), Geophys. Res. Lett., 22, 1449–1452, doi:10.1029/95GL01493, 1995.

Illman, W. A.: Analysis of permeability scaling within single boreholes, Geophys. Res. Lett., 31, l06503, doi:10.1029/2003GL019303, 2004.

Illman, W. A.: Hydraulic Tomography Offers Improved Imaging of Heterogeneity in Fractured Rocks, Groundwater, 52, 659–684, doi:10.1111/gwat.12119, 2014.

Illman, W. A. and Neuman, S. P.: Type-Curve Interpretation of Multirate Single-Hole Pneumatic Injection Tests in Unsaturated Fractured Rock, Ground Water, 38, 899–911, doi:10.1111/j.1745-6584.2000.tb00690.x, 2000.

Illman, W. A. and Tartakovsky, D. M.: Asymptotic analysis of cross-hole pneumatic injection tests in unsaturated fractured tuff, Adv. Water Resour., 28, 1217–1229, doi:10.1016/j.advwatres.2005.03.011, 2005.

Illman, W. A., Liu, X., Takeuchi, S., Yeh, T.-C. J., Ando, K., and Saegusa, H.: Hydraulic tomography in fractured granite: Mizunami Underground Research site, Japan, Water Resour. Res., 45, w01406, doi:10.1029/2007WR006715, 2009.

Julivert, M., Fontboté, J., Ribeiro, A., and Conde, L.: Marpa tectónico de la Península Ibérica y Baleares, E. 1:1000000, Tech. rep., IGME, http://info.igme.es/cartografiadigital/datos/tematicos/pdfs/MapaTectonico_1000.pdf (last access: 11 May 2016), 1972.

Jurado, M.: Estudios geológico-estructurales y geofísicos, Proyecto ratones, internal report: 10·cja·if·03, ENRESA, 1999.

Jurado, M.: Avance sobre evaluación de la testificatest geofísica de sondeos adquirida en mina Ratones., Proyecto ratones, internal report: 10·cja·ia·12, ENRESA, 2000.

Ko, N.-Y., Ji, S.-H., Koh, Y.-K., and Choi, J.-W.: Evaluation of two conceptual approaches for groundwater flow simulation for a rock domain at the block-scale for the Olkiluoto site, Finland, Eng. Geol., 193, 297–304, doi:10.1016/j.enggeo.2015.05.003, 2015.

Lee, J.-Y. and Lee, K.-K.: Analysis of the Quality of Parameter Estimates from Repeated Pumping and Slug Tests in a Fractured Porous Aquifer System in Wonju, Korea, Ground Water, 37, 692–700, doi:10.1111/j.1745-6584.1999.tb01161.x, 1999.

Long, J., Karasaki, K., Davey, A., Peterson, J., Landsfeld, M., Kemeny, J., and Martel, S.: An inverse approach to the construction of fracture hydrology models conditioned by geophysical data, Int. J. Rock Mech. Min., 28, 121–142, doi:10.1016/0148-9062(91)92162-R, 1991.

Long, J. C. S. and Billaux, D. M.: From field data to fracture network modeling: An example incorporating spatial structure, Water Resour. Res., 23, 1201–1216, doi:10.1029/WR023i007p01201, 1987.

Martí, D., Carbonell, R., Tryggvason, A., Escuder, J., and Pérez-Estaún, A.: Mapping brittle fracture zones in three dimensions: high resolution traveltime seismic tomography in a granitic pluton, Geophys. J. Int., 149, 95–105, doi:10.1046/j.1365-246X.2002.01615.x, 2002.

Martínez-Landa, L. and Carrera, J.: An analysis of hydraulic conductivity scale effects in granite (Full-scale Engineered Barrier Experiment (FEBEX), Grimsel, Switzerland), Water Resour. Res., 41, w03006, doi:10.1029/2004WR003458, 2005.

Martínez-Landa, L. and Carrera, J.: A methodology to interpret cross-hole tests in a granite block, J. Hydrol., 325, 222–240, doi:10.1016/j.jhydrol.2005.10.017, 2006.

Martínez-Landa, L., Alcahud, A., Jordan, J., and Carrera, J.: Modelo hidrogeológico del entorno de la mina Ratones (Albalá – Cáceres), Proyecto ratones, informe de proyecto: 10·upc·if·03, ENRESA, 2004.

Mauldon, A. D., Karasaki, K., Martel, S. J., Long, J. C. S., Landsfeld, M., Mensch, A., and Vomvoris, S.: An inverse technique for developing models for fluid flow in fracture systems using simulated annealing, Water Resour. Res., 29, 3775–3789, doi:10.1029/93WR00664, 1993.

Meier, P. M., Carrera, J., and Sánchez-Vila, X.: An evaluation of Jacob's Method for the interpretation of pumping tests in heterogeneous formations, Water Resour. Res., 34, 1011–1025, doi:10.1029/98WR00008, 1998.

Moreno, L. and Neretnieks, I.: Fluid flow and solute transport in a network of channels, J. Contam. Hydrol., 14, 163–192, doi:10.1016/0169-7722(93)90023-L, 1993.

Neuman, S. P.: Groundwater Flow and Quality Modelling, chap. Stochastic Continuum Representation of Fractured Rock Permeability as an Alternative to the REV and Fracture Network Concepts, Springer, the Netherlands, Dordrecht, doi:10.1007/978-94-009-2889-3_19, 331–362, 1988.

Ortuño, F., Floría, E., Carretero, G., and Suso, J.: Caracterización hidráulica de Mina Ratones, Proyecto ratones, internal report, rat·ait·ia·04, ENRESA, 2000.

Perez del Villar, L., Cózar, J., Pardillo, J., Pelayo, M., and Labajo, M.: Caracterización mineralógica y geoquímica de las harinas de falla y tapices de fractura del proyecto Ratones (Albalá, Cáceres), Proyecto ratones, internal report: 10·cie·if·3·99, ciemat/dieae/54211/6-99, ENRESA, 1999.

Pérez-Estaún, A.: Estudios geológicos-estructurales y Geofísicos en Mina Ratones, Proyecto ratones, internal report: 10·cja·if·03, ENRESA, 1999.

Pérez-Estaún, A., Carbonell, R., Matí, D., I., A., Jurado, M., Fernández, M., Marzán, I., and Escuder-Viruete, J.: Estudios geológico-estructurales y geofísicos en Mina Ratones (Plutón de Albalá), Publicación técnica de enresa 0512002, madrid, 211, ENRESA, 2002.

Rouleau, A. and Gale, J.: Statistical characterization of the fracture system in the Stripa granite, Sweden, Int. J. Rock Mech. Min., 22, 353–367, doi:10.1016/0148-9062(85)90001-4, 1985.

Sánchez-Vila, X., Carrera, J., and Girardi, J. P.: Scale effects in transmissivity, J. Hydrol., 183, 1–22, doi:10.1016/S0022-1694(96)80031-X, 1996.

Selroos, J.-O. and Follin, S.: Overview of hydrogeological site-descriptive modeling conducted for the proposed high-level nuclear waste repository site at Forsmark, Sweden, Hydrogeol. J., 22, 295–298, doi:10.1007/s10040-013-1077-x, 2013.

Shapiro, A. M. and Hsieh, P.: Research in fractured rock hydrogeology. Characterizing fluid movement and chemical transport in fractured rock at the Mirror Lake drainage basin, New Hampshire, Proceedings of the technical meeting, monterey, california, US Geological Survey toxic substance hydrology program, Reston, VA, http://pubs.er.usgs.gov/publication/wri914034, report, 1991.

Stephens, M., Follin, S., Petersson, J., Isaksson, H., Juhlin, C., and Simeonov, A.: Review of the deterministic modelling of deformation zones and fracture domains at the site proposed for a spent nuclear fuel repository, Sweden, and consequences of structural anisotropy, Tectonophysics, 653, 68–94, doi:10.1016/j.tecto.2015.03.027, 2015.

Stober, I.: Ergebnisse geohydraulischer und hydrochemischer Untersuchungen im kristallinen Grundgebirge des Schwarzwaldes und seiner, Randgebiete, in: Aquifersysteme Südwestdeutschlands – Eine Vorlesungsreihe an der Universität Tübingen, Tübinger Geowissenschaftliche Arbeiten (TGA), Herausgeber: Herbert, M. and Teutsch, G., Reihe C, 14 Abb., 1–17, 1997.

Svensson, U.: A continuum representation of fracture networks. Part I: Method and basic test cases, J. Hydrol., 250, 170–186, doi:10.1016/S0022-1694(01)00435-8, 2001a.

Svensson, U.: A continuum representation of fracture networks. Part II: application to the Äspö Hard Rock laboratory, J. Hydrol., 250, 187–205, doi:10.1016/S0022-1694(01)00436-X, 2001b.

Theis, C. V.: The relation between the lowering of the Piezometric surface and the rate and duration of discharge of a well using ground-water storage, Eos, Transactions American Geophysical Union, 16, 519–524, doi:10.1029/TR016i002p00519, 1935.

Tsang, Y. W., Tsang, C. F., Hale, F. V., and Dverstorp, B.: Tracer transport in a stochastic continuum model of fractured media, Water Resour. Res., 32, 3077–3092, doi:10.1029/96WR01397, 1996.

Vesselinov, V. V., Neuman, S. P., and Illman, W. A.: Three-dimensional numerical inversion of pneumatic cross-hole tests in unsaturated fractured tuff: 2. Equivalent parameters, high-resolution stochastic imaging and scale effects, Water Resour. Res., 37, 3019–3041, doi:10.1029/2000WR000135, 2001.